The Astrophysical Journal Letters, 934:L28 (7pp), 2022 August 1 https://doi.org/10.3847/2041-8213/ac7f28

Third and Fourth Harmonics of Electromagnetic Emissions by a Weak Beam in a Solar Wind Plasma with Random Density Fluctuations

C. Krafft and P. Savoini
Laboratoire de Physique des Plasmas (LPP), CNRS, Sorbonne Université, Observatoire de Paris, Université Paris-Saclay, Ecole polytechnique, Institut Polytechnique de Paris, F-91120 Palaiseau, France; catherine.krafft@universite-paris-saclay.fr
Received 2022 May 17; revised 2022 June 30; accepted 2022 June 30; published 2022 August 1

Abstract

Electromagnetic emissions $\mathcal{H}_3$ and $\mathcal{H}_4$ at the third and fourth harmonics of the plasma frequency ω_p were observed during the occurrence of type II and type III solar radio bursts. Two-dimensional particle-in-cell simulations are performed using a weak beam, high space and time resolutions, and a plasma with density fluctuations of a few percent, for parameters relevant to regions of type III bursts. For the first time, a detailed study of the different wave coalescence processes involved in the generation of $\mathcal{H}_3$ and $\mathcal{H}_4$ waves is presented and the impact of density fluctuations on the wave interaction mechanisms is demonstrated. Energy ratios between the second, third, and fourth harmonics $\mathcal{H}_2$, $\mathcal{H}_3$, and $\mathcal{H}_4$ are consistent with space observations. It is shown that, in both homogeneous and inhomogeneous plasmas, the dominant processes generating $\mathcal{H}_3$ ($\mathcal{H}_4$) are the coalescence of $\mathcal{H}_2$ ($\mathcal{H}_3$) with a Langmuir wave, in spite of the random density fluctuations modifying the waves' resonance conditions by energy transport in the wavevector space and of the damping of Langmuir waves. The role of the backscattered (forward-propagating) Langmuir waves coming from the first (second) cascade of the electrostatic decay of beam-driven Langmuir waves is determinant in these processes. Understanding such wave coalescence mechanisms can provide indirect information on Langmuir and ion acoustic wave turbulence, the average level of density inhomogeneities, and suprathermal electron fluxes generated in solar wind regions where the harmonics manifest. Causes for the rarity of their observations are discussed.

Unified Astronomy Thesaurus concepts: Solar electromagnetic emission (1490); Solar wind (1534); Radio bursts (1339)

1. Introduction

Electromagnetic emissions at the third harmonic of the plasma frequency ω_p have been reported during the occurrence of type II (Bakunin et al. 1990; Kliem et al. 1992; Zlotnik et al. 1998; Brazhenko et al. 2012) and type III solar radio bursts (Kundu 1965; Takakura & Yousef 1974; Zlotnik 1978; Cairns 1986; Reiner et al. 1992; Reiner & MacDowall 2019), even if rarely and sometimes controversially. The first unambiguous and clear observation of electromagnetic harmonics at $n\omega_p$ ($n = 3-5$) during type III bursts was performed by the satellite ISEE1 in the solar wind and Earth's foreshock region (Cairns 1986). Recently, the Wind spacecraft detected several events exhibiting third harmonic emissions in interplanetary type III bursts observed locally near 1 au (Reiner & MacDowall 2019). Missions such as Parker Solar Probe and Solar Orbiter should be able to detect locally generated type III harmonic emissions at $n\omega_p$ ($n > 2$) with intensities above the remote radiation (Reiner & MacDowall 2019).

In this Letter, we give evidence for the mechanisms of generation of the third $\mathcal{H}_3$ and fourth $\mathcal{H}_4$ electromagnetic harmonics, as well as the impact of background plasma density fluctuations on such emissions. Note that the difficulty in observing such waves, excluding the instrumental limitations, is partly due to the weakness of the electron beams generating Langmuir wave turbulence in the bursts' source regions and to the presence of plasma density irregularities, which can prevent wave–wave interactions from proceeding efficiently. To date, three main nonlinear processes have been proposed to explain the generation of $\mathcal{H}_3$ (e.g., Zheleznyakov & Zlotnik 1974; Zlotnik 1978; Cairns 1988; Yin et al. 1998; Zlotnik et al. 1998; Ziebell et al. 2015), i.e., (i)–(ii) the coalescences of the second electromagnetic (electrostatic) harmonic $\mathcal{H}_2$ ($\mathcal{L}_2$) with a Langmuir wave of frequency ω_p (Cairns 1986, 1988; Yi et al. 2007; Zlotnik et al. 1998), or (iii) the merging of three Langmuir waves (Zlotnik et al. 1998). For type III bursts, the last process is less effective (Zlotnik et al. 1998).

Using particle-in-cell (PIC) simulations, some authors studied the excitation, by a strong beam propagating in a homogeneous plasma, of electromagnetic and electrostatic harmonic waves emitted at $n\omega_p$ (up to $n = 4$) and discussed the possible mechanisms of generation (Rhee et al. 2009). Moreover, third harmonic excitation was also considered in the framework of electromagnetic weak turbulence theory (Ziebell et al. 2015). In the present work, 2D-PIC simulations are performed using a weak beam, high space and time resolutions, and an inhomogeneous plasma with density fluctuations of a few percent, as in the solar wind. For the first time, a detailed study of the role played by wave coalescence processes in the generation of $\mathcal{H}_3$ and $\mathcal{H}_4$ electromagnetic harmonics is presented and the impact of density fluctuations on these mechanisms is shown. Understanding such processes can provide indirect information on the population of nonthermal electrons, as well as the Langmuir and ion acoustic wave turbulence generated in source regions of harmonic waves.

2. Generation of Electromagnetic Harmonics

In a 2D simulation box of size $L_x \times L_y = 1448 \times 1448\lambda_D^2$, an electron beam with velocity $v_b = 0.25c$ and density

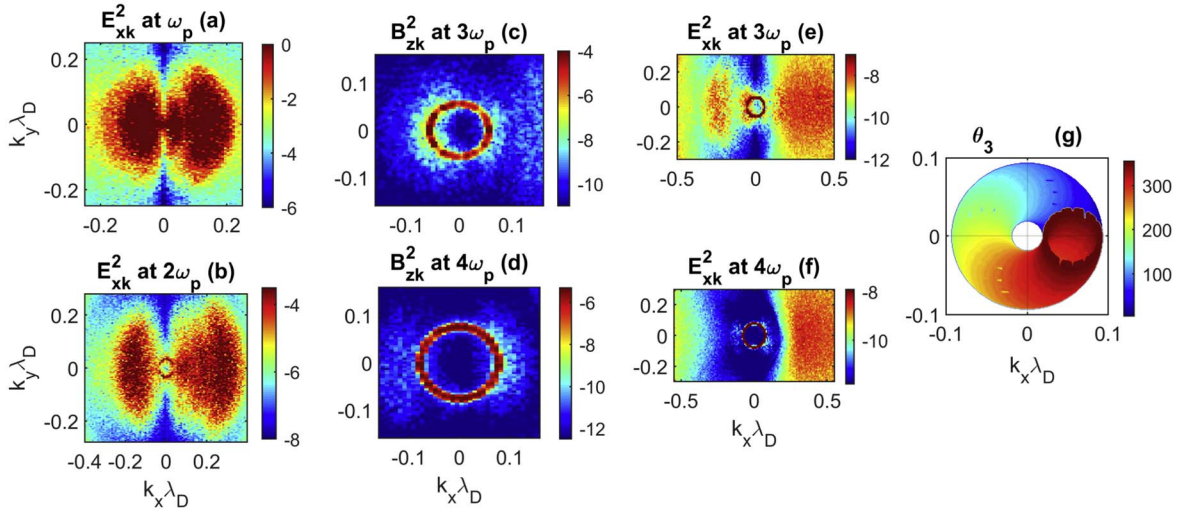

Figure 1. Homogeneous plasma ($\Delta N = 0$) at asymptotic time $\omega_p t = 8760$; ((a)-(f)): wave spectra in the plane (k_x, k_y); (g): resonance conditions in the plane (k_x, k_y). (a) $|E_{xk}|^2$ at $\omega_k \simeq \omega_p$, with Langmuir waves $\mathcal{L}$, $\mathcal{L}''$ ($k_x > 0$) and $\mathcal{L}'$ ($k_x < 0$). (b) $|E_{xk}|^2$ at $\omega_k \simeq 2\omega_p$, with electric field contribution to $\mathcal{H}_2$ (central ring) and electrostatic harmonics $\mathcal{L}_2$ ($k_{2x} > 0$) and $\mathcal{L}_2'$ ($k_{2x}' < 0$). (c) $|B_{zk}|^2$ at $\omega_k \simeq 3\omega_p$: wave $\mathcal{H}_3$. (d) $|B_{zk}|^2$ at $\omega_k \simeq 4\omega_p$: wave $\mathcal{H}_4$. (e) $|E_{xk}|^2$ at $\omega_k \simeq 3\omega_p$, with electric field contribution to $\mathcal{H}_3$ (central ring) and electrostatic harmonics $\mathcal{L}_3$ ($k_{3x} > 0$) and $\mathcal{L}_3'$ ($k_{3x}' < 0$). (f) $|E_{xk}|^2$ at $\omega_k \simeq 4\omega_p$, with electric field contribution to $\mathcal{H}_4$ (central ring) and electrostatic harmonics $\mathcal{L}_4$ ($k_{4x} > 0$) and $\mathcal{L}_4'$ ($k_{4x}' < 0$). (g) Angle θ_3 ($\cos\theta_3 = k_{3x}/k_3$) in degrees, as a function of k_x and k_y of the Langmuir waves $\mathcal{L}_1 = \mathcal{L}$, $\mathcal{L}'$, $\mathcal{L}''$, showing the loci where wavenumber resonance conditions are satisfied for $\mathcal{H}_2 + \mathcal{L}_1 \rightarrow \mathcal{H}_3$. All variables are normalized. (a)–(f): logarithmic scales; (g): linear scale.

$n_b/n_0 = 5 \times 10^{-4}$ (n_0 is the density of the background ions) propagating along the x-axis generates Langmuir wave turbulence in (i) an inhomogeneous plasma typical of type III bursts' regions in the solar wind, with background random density fluctuations δn of average level $\Delta N = \langle(\delta n/n_0)^2\rangle^{1/2} \simeq 0.05$ and wavelengths much larger than those of the Langmuir waves, and (ii) the same plasma but without the initially applied density fluctuations. The 2D3V version of the code SMILEI (Derouillat et al. 2018) is used to provide calculations over almost 10^4 plasma periods. Details on the physical and numerical parameters were given in recent papers (Krafft & Savoini2021, 2022).

The beam radiates Langmuir waves $\mathcal{L}$ at frequency $\omega_k \simeq \omega_p$, which are in turn involved in two cascades of electrostatic decay, i.e., $\mathcal{L} \rightarrow \mathcal{L}' + \mathcal{S}'$ and $\mathcal{L}' \rightarrow \mathcal{L}'' + S''$, where $\mathcal{L}'$ and $\mathcal{L}''$ (S' and S'') are backscattered and forward-propagating Langmuir (ion acoustic) waves, respectively. Meanwhile, electrostatic harmonics of these high-frequency waves are produced, designated below as $\mathcal{L}_n$, $\mathcal{L}_n'$, and $\mathcal{L}''_n$, with n indicating the frequency $n\omega_p$ at which they are excited. Figure 1(a) presents the spectral electric energy density $|E_{xk}|^2$ at $\omega_k \simeq \omega_p$, in a homogeneous plasma and at asymptotic times, showing the beam-driven Langmuir waves $\mathcal{L}$ ($k_x\lambda_D \gtrsim 0.06$), the backscattered waves $\mathcal{L}'$ ($k_x < 0$), and the forward-propagating waves $\mathcal{L}''$ ($0.02 \lesssim k_x\lambda_D \lesssim 0.06$) (see also Krafft et al. 2015).

Three main nonlinear wave processes were proposed to explain the generation of the harmonics $\mathcal{H}_n$ ($n \geqslant 3$): (i) the fusion of n Langmuir waves and (ii)–(iii) the coalescence of the $(n-1)^{th}$ electrostatic (electromagnetic) harmonic wave $\mathcal{L}_{n-1}$ ($\mathcal{H}_{n-1}$) with a Langmuir wave, i.e., the process $\mathcal{L}_{n-1} + \mathcal{L}_1 \rightarrow \mathcal{H}_n$ ($\mathcal{H}_{n-1} + \mathcal{L}_1 \rightarrow \mathcal{H}_n$) (Cairns 1988; Yin et al. 1998; Zlotnik et al. 1998), where $\mathcal{L}_1$ designates $\mathcal{L}$, $\mathcal{L}'$, or $\mathcal{L}''$. For type III bursts, the first process is supposed to be very weak, whereas the third one, $\mathcal{H}_{n-1} + \mathcal{L}_1 \rightarrow \mathcal{H}_n$, should be dominant compared to the second one (Zlotnik et al. 1998). However, no convincing proof of such assumptions and no description of the contributions of each coalescence channel to the generation of $\mathcal{H}_3$ and $\mathcal{H}_4$ have been provided to date for type III bursts.

Electromagnetic emissions at frequencies $n\omega_p$ ($n \geqslant 1$) are clearly observed in the simulations presented hereafter, when the plasma is homogeneous or contains external density fluctuations with $\Delta N \simeq 0.05$. Figures 1(c)–(d) show, at asymptotic times, the spectral electromagnetic energy density $|B_{zk}|^2$ in the plane (k_x, k_y), at $\omega_k \simeq n\omega_p$ ($n = 3, 4$) and $\Delta N = 0$ (homogeneous case). Note that the spectra are consistent with those obtained by Rhee et al. (2009). The dispersion relations $\omega_{k_n}^2 = \omega_p^2 + k_n^2 c^2$ of the $\mathcal{H}_n$ waves appear as circular rings, with the wavevector moduli k_n matching the theoretical values $k_{n,th}\lambda_D = (n^2-1)^{1/2} v_T/c$ ($k_{3,th}\lambda_D \simeq 0.056$, $k_{4,th}\lambda_D \simeq 0.077$); v_T is the plasma thermal velocity. These distributions exhibit some angular dependence; for $n = 3$, the intensity is maximum within a cone $110° \lesssim \theta_3 \lesssim 250°$ ($\cos\theta_3 = k_{3x}/k_3$), corresponding to waves propagating with a negative parallel wavenumber $k_{3x} < 0$, which can be observed starting from $\omega_p t \simeq 4000$; those can only be produced, according to the wavevectors' resonance conditions of the process $\mathcal{H}_2 + \mathcal{L}_1 \rightarrow \mathcal{H}_3$, when $\mathcal{L}_1 = \mathcal{L}'$. In a plasma with density fluctuations, the waves $\mathcal{L}'$ also arise from transformations of the waves $\mathcal{L}$ on inhomogeneities. A smaller enhancement is visible for $-45° \lesssim \theta_3 \lesssim 45°$, i.e., for $\mathcal{H}_3$ waves with $k_{3x} > 0$, (Figure 1(c)), due to the contribution at late times of waves $\mathcal{L}''$ (see also Figure 2(e)). Figure 1(g) shows the loci where the resonance conditions for the wavevectors involved in the process $\mathcal{H}_2 + \mathcal{L}_1 \rightarrow \mathcal{H}_3$ can be satisfied, i.e., the angle θ_3 as a function of the wavenumbers k_x and k_y of the Langmuir waves $\mathcal{L}_1$. When $110° \lesssim \theta_3 \lesssim 250°$ ($-45° \lesssim \theta_3 \lesssim 45°$), resonance conditions are only possible if $k_x < 0$ ($0 < k_x\lambda_D \lesssim 0.06$), i.e., for $\mathcal{L}_1 = \mathcal{L}'$ ($\mathcal{L}_1 = \mathcal{L}''$), in agreement with Figure 1(c).

For $n = 4$ (Figure 1(d)), the spectrum of $\mathcal{H}_4$ exhibits a quasi-uniform distribution with a larger wave intensity within $-45° \lesssim \theta_4 \lesssim 45°$. Moreover, electrostatic harmonics $\mathcal{L}_n$ and $\mathcal{L}_n'$ are also observed in Figures 1(b), (e)–(f) that present $|E_{xk}|^2$ at $\omega_k \simeq n\omega_p$ ($n = 2, 3, 4$); one observes therein, between the electrostatic emissions at larger $|k_x|$, a circular ring at small k_x representing the electric contribution to $\mathcal{H}_n$. The role of the waves $\mathcal{L}_{2,3}$ and $\mathcal{L}_{2,3}'$ in the generation of the harmonics $\mathcal{H}_{3,4}$ is discussed below.

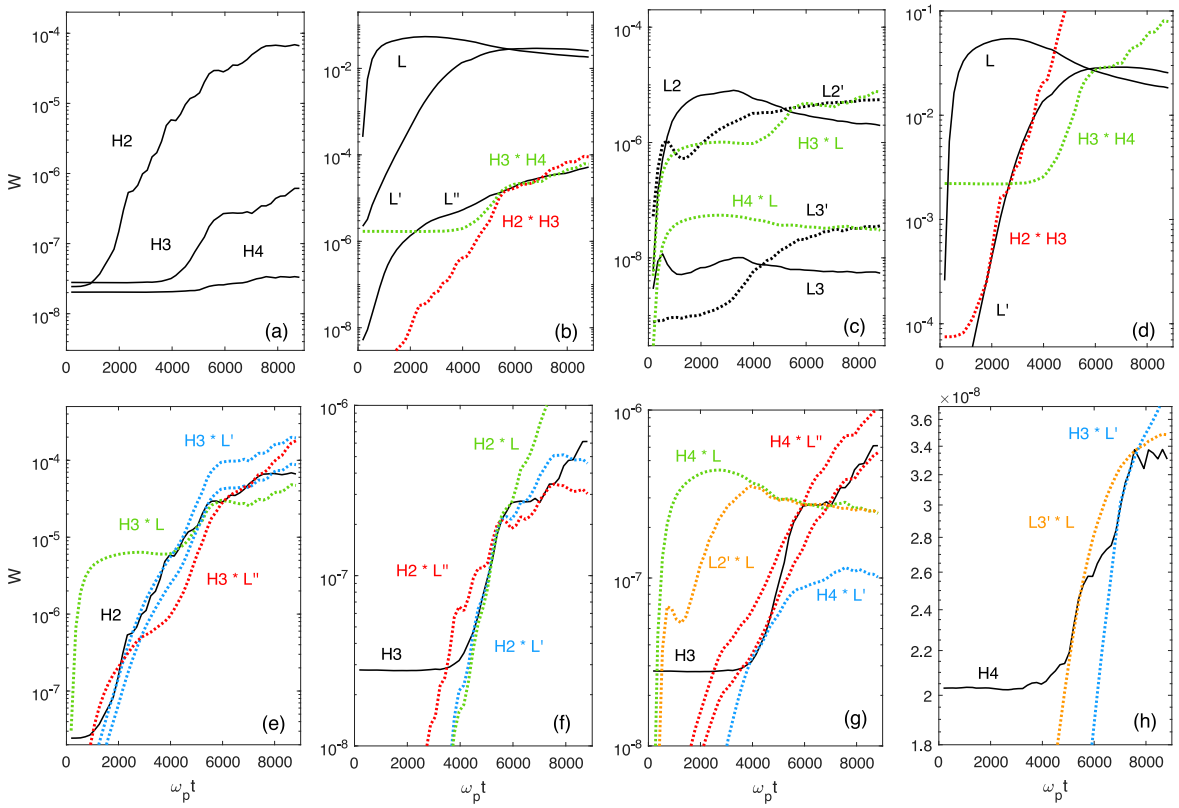

Figure 2. Homogeneous plasma: time variations of wave energies (black curves) and products between them (color curves). (a)–(g): logarithmic scale; (h): linear scale. (a) Time variations of $W_{\mathcal{H}_2}$, $W_{\mathcal{H}_3}$, and $W_{\mathcal{H}_4}$ (black). (b) Time variations of $W_{\mathcal{L}}$, $W_{\mathcal{L}'}$, and $W_{\mathcal{L}''}$ (black), and of $W_{\mathcal{H}_3}W_{\mathcal{H}_4}$ and $W_{\mathcal{H}_2}W_{\mathcal{H}_3}$, labeled by $H_3{}^*H_4$ (green) and $H_2{}^*H_3$ (red). (c) Time variations of $W_{\mathcal{L}_2}$ and $W_{\mathcal{L}_3}$ (solid black), $W_{\mathcal{L}'_2}$ and $W_{\mathcal{L}'_3}$ (dotted black), and $W_{\mathcal{H}_3}W_{\mathcal{L}}$ and $W_{\mathcal{H}_4}W_{\mathcal{L}}$, labeled by $H_3{}^*L$ (green) and $H_4{}^*L$ (green). (d) Time variations of $W_{\mathcal{L}}$ and $W_{\mathcal{L}'}$ (black), $W_{\mathcal{H}_3}W_{\mathcal{H}_4}$, and $W_{\mathcal{H}_2}W_{\mathcal{H}_3}$, labeled by $H_3{}^*H_4$ (green) and $H_2{}^*H_3$ (red). (e) Time variations of $W_{\mathcal{H}_2}$ (black), as well as $W_{\mathcal{H}_3}W_{\mathcal{L}}$, $W_{\mathcal{H}_3}W_{\mathcal{L}'}$, and $W_{\mathcal{H}_3}W_{\mathcal{L}''}$, labeled by $H_3{}^*L$ (green), $H_3{}^*L'$ (blue), and $H_3{}^*L''$ (red); the blue curve is duplicated (i.e., multiplied by another coupling factor) to show the relation $W_{\mathcal{H}_2} \propto W_{\mathcal{H}_3}W_{\mathcal{L}'}$ occurring at different times. (f) Time variations of $W_{\mathcal{H}_3}$ (black), as well as $W_{\mathcal{H}_2}W_{\mathcal{L}}$, $W_{\mathcal{H}_2}W_{\mathcal{L}'}$ and $W_{\mathcal{H}_2}W_{\mathcal{L}''}$, labeled by $H_2{}^*L$ (green), $H_2{}^*L'$ (blue), and $H_2{}^*L''$ (red). (g) Time variations of $W_{\mathcal{H}_3}$ (black), as well as $W_{\mathcal{H}_4}W_{\mathcal{L}}$, $W_{\mathcal{H}_4}W_{\mathcal{L}'}$, $W_{\mathcal{H}_4}W_{\mathcal{L}''}$ and $W_{\mathcal{L}'_2}W_{\mathcal{L}}$, labeled by $H_4{}^*L$ (green), $H_4{}^*L'$ (blue), $H_4{}^*L''$ (red) and $L_2'{}^*L$ (orange); the red curve is duplicated (i.e., multiplied by another coupling factor) to show the relation $W_{\mathcal{H}_3} \propto W_{\mathcal{H}_4}\, W_{\mathcal{L}''}$ occurring at different times. (h) Time variations of $W_{\mathcal{H}_4}$ (black), $W_{\mathcal{H}_3}W_{\mathcal{L}'}$ and $W_{\mathcal{L}'_3}W_{\mathcal{L}}$, labeled by $H_3{}^*L'$ (blue) and $L_3'{}^*L$ (orange); the two latter curves are smoothed, due to oscillations. Energies are normalized by the initial beam kinetic energy.

Figure 2(a) presents the time variations of the magnetic energies $W = (1/2)\iint B^2(x,\, y)dxdy$ of the waves $\mathcal{H}_2$, $\mathcal{H}_3$, and $\mathcal{H}_4$ (see also Krafft & Savoini 2021, 2022). They reach asymptotically the levels $W_{\mathcal{H}_3} \simeq 0.01 W_{\mathcal{H}_2}$ and $W_{\mathcal{H}_4} \simeq 0.05 W_{\mathcal{H}_3}$, which are consistent with observations of type III bursts (Cairns 1986) and estimates obtained in the framework of weak turbulence theory (Ziebell et al. 2015). Figure 2(b) and (c) show the time evolution of the energies $W = (1/2)\iint E^2(x,\, y)dxdy$ of the Langmuir waves $\mathcal{L}$, $\mathcal{L}'$, and $\mathcal{L}''$, as well as of the harmonic waves $\mathcal{L}_2$, $\mathcal{L}'_2$ and $\mathcal{L}_3$, $\mathcal{L}'_3$. In order to find resonant interactions between these waves leading to the generation of $\mathcal{H}_3$ and $\mathcal{H}_4$ waves, we search proportionality relations like $W_{\mathcal{H}_i}(t) \propto W_{\mathcal{H}_j}(t) W_{\mathcal{L}_k}(t)$, with $i,\, j = 2,\, 3,\, 4;\, i \neq j$; and $k = 1,\, 2,\, 3$. In order to provide clear evidence owing to the curves' superimposition, products $W_{\mathcal{H}_j}(t) W_{\mathcal{L}_k}(t)$ are multiplied by a coefficient proportional to the waves' coupling factors. For simplicity, we suppress below in our notations the time dependency. For a given interaction process (e.g., $\mathcal{H}_2 + \mathcal{L}_1 \rightarrow \mathcal{H}_3$, $\mathcal{L}_1 = \mathcal{L},\, \mathcal{L}',\, \mathcal{L}''$), we have to find all possible time intervals where the relations $W_{\mathcal{H}_2} \propto W_{\mathcal{H}_3}W_{\mathcal{L}_1}$, $W_{\mathcal{H}_3} \propto W_{\mathcal{H}_2}W_{\mathcal{L}_1}$, and $W_{\mathcal{L}_1} \propto W_{\mathcal{H}_2}W_{\mathcal{H}_3}$ are satisfied, taking into account that beforehand resonance conditions for frequencies and wavevectors should be fulfilled (e.g., Figure 1(g)). Note that during the time evolution, the waves $\mathcal{H}_{3,4}$ can interact successively and/or simultaneously with several different pairs of waves, and thus the number of possibilities to search for is large.

One can see in Figure 2(d) that $W_{\mathcal{L}'} \propto W_{\mathcal{H}_2}W_{\mathcal{H}_3}$ during the time range $\Delta T \simeq [1700\text{–}3600]\omega_p^{-1}$, whereas $W_{\mathcal{H}_2} \propto W_{\mathcal{H}_3}W_{\mathcal{L}'}$ and $W_{\mathcal{H}_3} \propto W_{\mathcal{H}_2}W_{\mathcal{L}'}$ can be observed in Figures 2(e)–(f) within $[1700\text{–}4500]\omega_p^{-1}$ and $[4600\text{–}5600]\omega_p^{-1}$, respectively. This shows the occurrence of the process $\mathcal{H}_2 + \mathcal{L}' \longrightarrow \mathcal{H}_3$ during the stage of growth of $\mathcal{H}_3$, which is coherent with the spectral enhancements at $k_{3x} < 0$ observed in Figure 1(c), as $k_{3x} = k_{2x} + k_{\mathcal{L}'x} = k_{2x} - |k_{\mathcal{L}'x}|$ is mostly negative, according to the ranges of values of the wavenumbers ($\boldsymbol{k}_{\mathcal{L}'}$ is the wavevector of $\mathcal{L}'$). However, other Langmuir waves also contribute to this coalescence, as $W_{\mathcal{L}''} \propto W_{\mathcal{H}_2}W_{\mathcal{H}_3}$ within $[5400\text{–}7000]\omega_p^{-1}$ (Figure 2(b)), $W_{\mathcal{H}_2} \propto W_{\mathcal{H}_3}W_{\mathcal{L}''}$ within $[6300\text{–}7700]\omega_p^{-1}$ (Figure 2(e)), and $W_{\mathcal{H}_3} \propto W_{\mathcal{H}_2}W_{\mathcal{L}''}$ within $[4800\text{–}5800,\, 7000\text{–}7500]\omega_p^{-1}$ (Figure 2(f)); the corresponding coalescence $\mathcal{H}_2 + \mathcal{L}'' \longrightarrow \mathcal{H}_3$ occurs mainly within the range $4800 \lesssim \omega_p t \lesssim 7500$ and thus participates to the energy growth of $\mathcal{H}_3$ waves at later times. The waves $\mathcal{L}$ play a smaller role, at times when their amplitudes reach those of the waves $\mathcal{L}'$, i.e., $4500 \lesssim \omega_p t \lesssim 5500$, as $W_{\mathcal{H}_2} \propto W_{\mathcal{H}_3}W_{\mathcal{L}}$ and $W_{\mathcal{H}_3} \propto W_{\mathcal{H}_2}W_{\mathcal{L}}$ are found, during $[4000\text{–}6000]\omega_p^{-1}$ and $[4500 - 5800]\omega_p^{-1}$, respectively (Figures 2(e)–(f)); in this case, the waves $\mathcal{H}_2$ have to

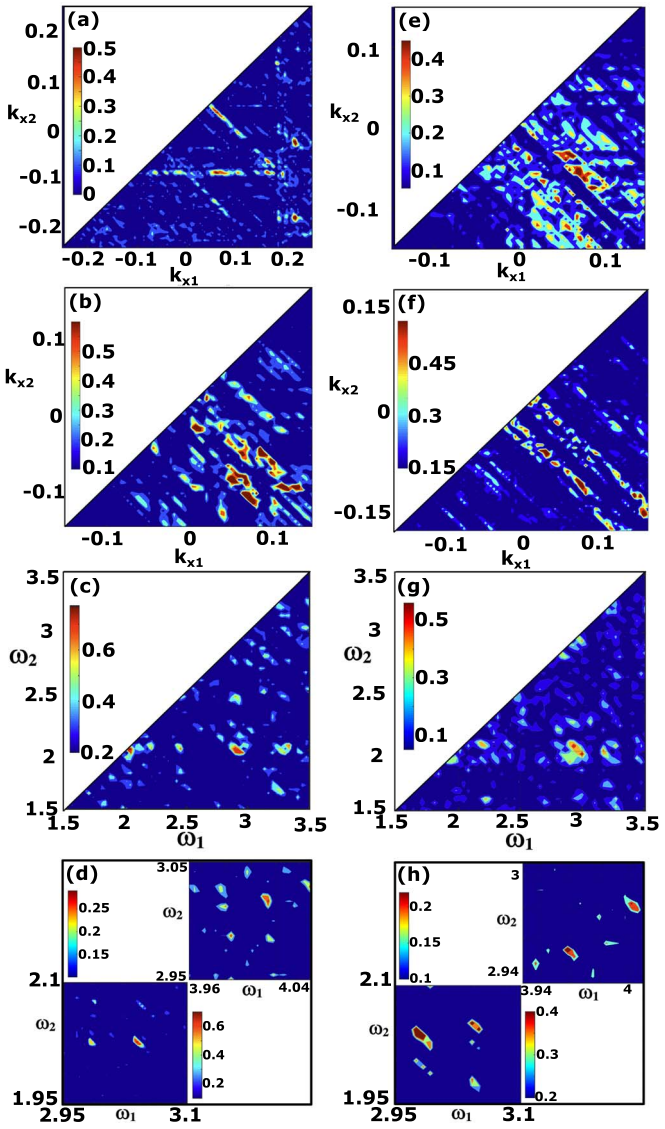

Figure 3. Examples of cross sections of the auto- and cross-bicoherences b_c of the magnetic and electric fields in the parallel wavenumber and frequency planes. The left (right) column refers to homogeneous (inhomogeneous) plasma. For each panel, the bottom shows the maxima of bicoherence (b_c), their location in frequency (ω_1, ω_2) and wavenumber (k_{x1}, k_{x2}) spaces, and the corresponding coalescence processes. Note that, as mentioned in the text, theory provides for our parameters the following values for the wavevectors' moduli of $\mathcal{H}_2$, $\mathcal{H}_3$, and $\mathcal{H}_4$: $k_2\lambda_D \simeq 0.035$, $k_3\lambda_D \simeq 0.056$, $k_4\lambda_D \simeq 0.077$. Note that for $\Delta N = 0.05$, spectral broadening due to density fluctuations can shift wavenumbers from their theoretical values. (a) $\Delta N = 0$, $\omega_p t = 3292$, $b_c \simeq 0.75$, ($k_{x1} \simeq 0.217$, $k_{x2} \simeq -0.187$), $\mathcal{L}(k_{x1}) + \mathcal{L}'(k_{x2}) \longrightarrow \mathcal{H}_2(k_{x1} + k_{x2} \simeq 0.03)$; $b_c \simeq 0.6$, ($k_{x1} \simeq 0.0564$, $k_{x2} \simeq 0.0347$), $\mathcal{H}_2(k_{x2}) + \mathcal{L}'(-k_{x1} - k_{x2} \simeq -0.091) \longrightarrow \mathcal{H}_3(-k_{x1})$. (b) $\Delta N = 0$, $\omega_p t = 4867$, $b_c = 0.9$, ($k_{x1} \simeq 0.074$, $k_{x2} \simeq -0.11$), $\mathcal{L}(k_{x1}) + \mathcal{L}'(k_{x2}) \longrightarrow \mathcal{H}_2(k_{x1} + k_{x2} \simeq -0.036)$; $b_c = 0.76$, ($k_{x1} \simeq 0.134$, $k_{x2} \simeq -0.099$), $\mathcal{L}(k_{x1}) + \mathcal{L}'(k_{x2}) \longrightarrow \mathcal{H}_2(k_{x1} + k_{x2} \simeq 0.035)$; $b_c \simeq 0.62$, ($k_{x1} \simeq 0.0911$, $k_{x2} \simeq -0.0564$), $\mathcal{H}_2(k_{x2} + k_{x1} \simeq 0.035) + \mathcal{L}'(-k_{x1}) \longrightarrow \mathcal{H}_3(k_{x2})$; $b_c = 0.7$ ($k_{x1} \simeq 0.052$, $k_{x2} \simeq -0.078$), $\mathcal{H}_3(k_{x1}) + \mathcal{L}'(k_{x2} - k_{x1} \simeq -0.13) \longrightarrow \mathcal{H}_4(k_{x2})$. (c) $\Delta N = 0$, $\omega_p t = 2743$, $b_c = 0.7$, ($\omega_1 = 2.93$, $\omega_2 = 2.01$), $\mathcal{H}_2(\omega_2) + \mathcal{L}' \longrightarrow \mathcal{H}_3(\omega_1)$. (d) $\Delta N = 0$, $\omega_p t = 4858$; (bottom): $b_c = 0.76$, ($\omega_1 = 3.02$, $\omega_2 = 2.00$), $\mathcal{H}_2(\omega_2) + \mathcal{L}_1 \longrightarrow \mathcal{H}_3(\omega_1)$; (top): $b_c = 0.32$, ($\omega_1 = 4.01$, $\omega_2 = 3.01$), $\mathcal{H}_3(\omega_2) + \mathcal{L}_1 \longrightarrow \mathcal{H}_4(\omega_1)$. (e) $\Delta N = 0.05$, $\omega_p t = 2369$, $b_c = 0.56$, ($k_{x1} \simeq 0.0564$, $k_{x2} \simeq -0.031$), $\mathcal{H}_2(-k_{x2}) + \mathcal{L}'(-k_{x1} + k_{x2} \simeq -0.087) \longrightarrow \mathcal{H}_3(-k_{x1})$; $b_c \simeq 0.51$, ($k_{x1} \simeq 0.06$, $k_{x2} \simeq -0.035$), $\mathcal{L}(k_{x2} + k_{x1} \simeq 0.025) + \mathcal{L}'(-k_{x1}) \longrightarrow \mathcal{H}_2(k_{x2})$. (f) $\Delta N = 0.05$, $\omega_p t = 3917$, $b_c = 0.85$, ($k_{x1} \simeq 0.161$, $k_{x2} \simeq -0.126$), $\mathcal{L}(k_{x1}) + \mathcal{L}'(k_{x2}) \longrightarrow \mathcal{H}_2(k_{x1} + k_{x2} \simeq 0.035)$; $b_c = 0.78$, ($k_{x1} \simeq 0.0347$, $k_{x2} \simeq -0.065$), $\mathcal{H}_2(k_{x1}) + \mathcal{L}'(-k_{x1} + k_{x2} \simeq -0.099) \longrightarrow \mathcal{H}_3(k_{x2})$; $b_c = 0.52$, ($k_{x1} \simeq 0.047$, $k_{x2} \simeq -0.078$), $\mathcal{H}_3(k_{x1}) + \mathcal{L}'(-k_{x1} + k_{x2} \simeq -0.125) \longrightarrow \mathcal{H}_4(k_{x2})$. (g) $\Delta N = 0.05$, $\omega_p t = 2108$, $b_c = 0.4$, ($\omega_1 = 3.00$, $\omega_2 = 2.01$), $\mathcal{H}_2(\omega_2) + \mathcal{L}_1 \longrightarrow \mathcal{H}_3(\omega_1)$.(h) $\Delta N = 0.05$, $\omega_p t = 4421$; (bottom): $b_c = 0.6$, ($\omega_1 = 2.97$, $\omega_2 = 1.98$), $\mathcal{H}_2(\omega_2) + \mathcal{L}_1 \longrightarrow \mathcal{H}_3(\omega_1)$; (top): $b_c = 0.4$, ($\omega_1 = 3.96$, $\omega_2 = 2.95$), $\mathcal{H}_3(\omega_2) + \mathcal{L}_1 \longrightarrow \mathcal{H}_4(\omega_1)$. All variables are normalized.

satisfy $k_{2x} < 0$ and $k_{\mathcal{L}x}$ has to belong to the smallest parallel wavenumbers of the waves $\mathcal{L}$ for the process $\mathcal{H}_2 + \mathcal{L} \longrightarrow \mathcal{H}_3$ to take place, reducing its probability of occurrence. In some time ranges, $\mathcal{H}_2$ and $\mathcal{H}_3$ interact with the three Langmuir waves $\mathcal{L}_1$ simultaneously; then, for example, interactions within the triplet ($\mathcal{H}_2$, $\mathcal{H}_3$, $\mathcal{L}'$) modify the exchanges of energy within the triplets ($\mathcal{H}_2$, $\mathcal{H}_3$, $\mathcal{L}$) and ($\mathcal{H}_2$, $\mathcal{H}_3$, $\mathcal{L}''$), not to mention interactions with the beam electrons; meanwhile, the decays $\mathcal{L} \rightarrow \mathcal{L}' + \mathcal{S}'$ and $\mathcal{L}' \rightarrow \mathcal{L}'' + \mathcal{S}''$ also occur, which transport part of the energy to low frequencies. Then, Langmuir wave energy is shared with several waves simultaneously. This circumstance makes the existence of the proportionality relations found within large time intervals very convincing. Thus, one can state that $\mathcal{H}_2$ waves coalesce with different Langmuir waves, depending on time, to generate the $\mathcal{H}_3$ waves; the waves $\mathcal{L}'$ play the most important role, as mentioned above regarding Figures 1(c) and (g).

Moreover, coalescence of $\mathcal{L}_1$ with $\mathcal{L}'_{n>1}$ waves also occurs. One finds that $W_{\mathcal{L}'_2} \propto W_{\mathcal{H}_3} W_{\mathcal{L}}$ within $5500 \lesssim \omega_p t \lesssim 8000$ (Figure 2(c)) and that $W_{\mathcal{H}_3} \propto W_{\mathcal{L}'_2} W_{\mathcal{L}}$ within a in a shorter time range (Figure 2(g)), but the relation $W_{\mathcal{L}} \propto W_{\mathcal{L}'_2} W_{\mathcal{H}_3}$ cannot be found. In turn, the wave $\mathcal{L}'_3$ plays a role in the growth of $\mathcal{H}_4$, via the coalescence channel $\mathcal{L}'_3 + \mathcal{L} \longrightarrow \mathcal{H}_4$, as $W_{\mathcal{L}'_3} \propto W_{\mathcal{H}_4} W_{\mathcal{L}}$ within $[6800\text{–}9000]\omega_p^{-1}$ (Figure 2(c)) and $W_{\mathcal{H}_4} \propto W_{\mathcal{L}'_3} W_{\mathcal{L}}$ within $[5000\text{–}5600]\omega_p^{-1}$ (Figure 2(h)).

For $\omega_p t \gtrsim 4000$, the coalescence $\mathcal{H}_3 + \mathcal{L}' \longrightarrow \mathcal{H}_4$ occurs as $W_{\mathcal{H}_3} \propto W_{\mathcal{H}_4} W_{\mathcal{L}'}$ within $[4000\text{–}4700]\omega_p^{-1}$ (Figure 2(g)), $W_{\mathcal{L}'} \propto W_{\mathcal{H}_3} W_{\mathcal{H}_4}$ within $[6100\text{–}6700]\omega_p^{-1}$ (Figure 2(d)) and $W_{\mathcal{H}_4} \propto W_{\mathcal{H}_3} W_{\mathcal{L}'}$ within $[6800\text{–}7500]\omega_p^{-1}$ (Figure 2(h)) are satisfied. The process $\mathcal{H}_3 + \mathcal{L}'' \longrightarrow \mathcal{H}_4$ takes place within $5400 \lesssim \omega_p t \lesssim 8800$, as $W_{\mathcal{L}''} \propto W_{\mathcal{H}_3} W_{\mathcal{H}_4}$ (Figure 2(b)) and $W_{\mathcal{H}_3} \propto W_{\mathcal{H}_4} W_{\mathcal{L}''}$ (Figure 2(g)) during this time interval, whereas $\mathcal{H}_3 + \mathcal{L} \longrightarrow \mathcal{H}_4$ occurs only during the time range $5900 \lesssim \omega_p t \lesssim 6800$ (Figure 2(g)).

In conclusion, if for the generation of $\mathcal{H}_3$ the coalescence $\mathcal{H}_2 + \mathcal{L}_1 \longrightarrow \mathcal{H}_3$ is clearly dominant, the process $\mathcal{L}'_2 + \mathcal{L} \longrightarrow \mathcal{H}_3$ also occurs. Moreover, the process $\mathcal{H}_3 + \mathcal{L}_1 \longrightarrow H_4$ ($\mathcal{L}'_3 + \mathcal{L}_1 \longrightarrow \mathcal{H}_4$) certainly (likely) takes place, where $\mathcal{L}_1 = \mathcal{L}'$, $\mathcal{L}''$ ($\mathcal{L}_1 = \mathcal{L}$, $\mathcal{L}'$). Moreover, examples of cross sections of the auto- and cross-bicoherence b_c calculated using the magnetic and electric fields are shown in the parallel wavenumber (k_{x1}, k_{x2}) and frequency (ω_1, ω_2) spaces in the left column of Figure 3. Most wave coalescence processes shown in Figure 2 present significant levels of b_c, in the time intervals where they appear, supporting the above results.

3. Impact of Density Fluctuations

When the plasma is randomly inhomogeneous, one expects significant changes compared to the results obtained above for a homogeneous plasma. Indeed, at times when the harmonics $\mathcal{H}_3$ and $\mathcal{H}_4$ grow, the Langmuir waves $\mathcal{L}_1$, $\mathcal{L}_n$, and $\mathcal{L}'_n$ damp (Figures 4(b)–(c)) so that the probability of efficient wave–wave interactions decreases. Figure 4(a) shows the time variations of the magnetic energies of the waves $\mathcal{H}_2$, $\mathcal{H}_3$, and $\mathcal{H}_4$, with asymptotic amplitudes $W_{\mathcal{H}_3} \simeq 0.006 W_{\mathcal{H}_2}$ and $W_{\mathcal{H}_4} \simeq 0.5 W_{\mathcal{H}_3}$ presenting orders of magnitude compatibility with those reported during type III bursts' observations (Cairns 1986).

The corresponding spectra are presented at asymptotic times for $\omega_k \simeq n\omega_p$ in Figures 5(a)–(f) (compare with Figures 1(a)–(f));

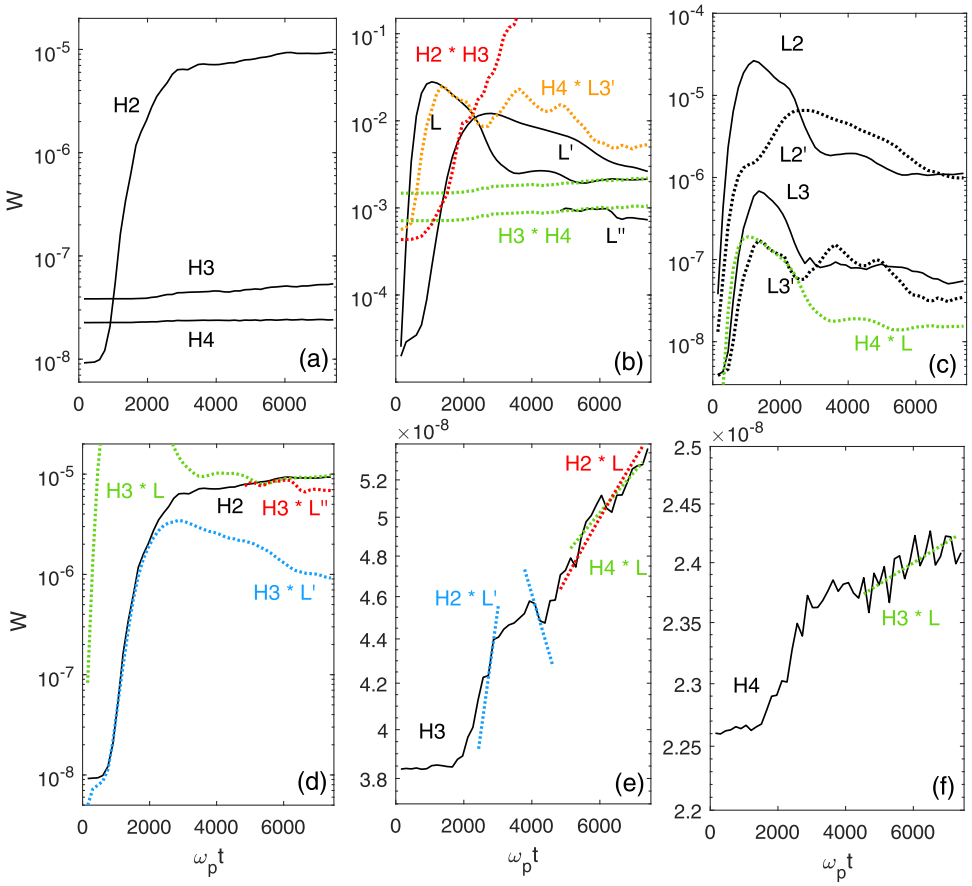

Figure 4. Inhomogeneous plasma ($\Delta N = 0.05$): time variations of wave energies (black curves) and products between them (color curves). (a)–(d): logarithmic scales; (e)–(f): linear scales. (a) Time variations of $W_{\mathcal{H}_2}$, $W_{\mathcal{H}_3}$, and $W_{\mathcal{H}_4}$ (black). (b) Time variations of $W_{\mathcal{L}}$, $W_{\mathcal{L}'}$, and $W_{\mathcal{L}''}$ for $\omega_p t > 4800$ (black), and of $W_{\mathcal{H}_3}W_{\mathcal{H}_4}$, $W_{\mathcal{H}_2}W_{\mathcal{H}_3}$, and $W_{\mathcal{H}_4}W_{\mathcal{L}'_3}$, labeled by $H_3 * H_4$ (green), $H_2 * H_3$ (red), and $H_4 * L'_3$ (orange); the green curve is duplicated to show both $W_{\mathcal{L}} \propto W_{\mathcal{H}_3}W_{\mathcal{H}_4}$ and $W_{\mathcal{L}''} \propto W_{\mathcal{H}_3}W_{\mathcal{H}_4}$. (c) Time variations of $W_{\mathcal{L}_2}$ and $W_{\mathcal{L}_3}$ (solid black), $W_{\mathcal{L}'_2}$ and $W_{\mathcal{L}'_3}$ (dotted black), and $W_{\mathcal{H}_4}W_{\mathcal{L}}$, labeled by $H_4 * L$ (green). (d) Time variations of $W_{\mathcal{H}_2}$ (black), $W_{\mathcal{H}_3}W_{\mathcal{L}}$, $W_{\mathcal{H}_3}W_{\mathcal{L}'}$, and $W_{\mathcal{H}_3}W_{\mathcal{L}''}$, labeled by $H_3 * L$ (green), $H_3 * L'$ (blue), and $H_3 * L''$ (red). (e) Time variations of $W_{\mathcal{H}_3}$ (black), $W_{\mathcal{H}_2}W_{\mathcal{L}}$, $W_{\mathcal{H}_2}W_{\mathcal{L}'}$, and $W_{\mathcal{H}_4}W_{\mathcal{L}}$, labeled by $H_2 * L$ (red), $H_2 * L'$ (blue), and $H_4 * L$ (green); the green (red) straight line results from the linear interpolation of $W_{\mathcal{H}_4}W_{\mathcal{L}}$ ($W_{\mathcal{H}_2}W_{\mathcal{L}}$). (f) Time variations of $W_{\mathcal{H}_4}$ (black) and $W_{\mathcal{H}_3}W_{\mathcal{L}}$, interpolated by a green line labeled by $H_3 * L$. Energies are normalized by the initial beam kinetic energy.

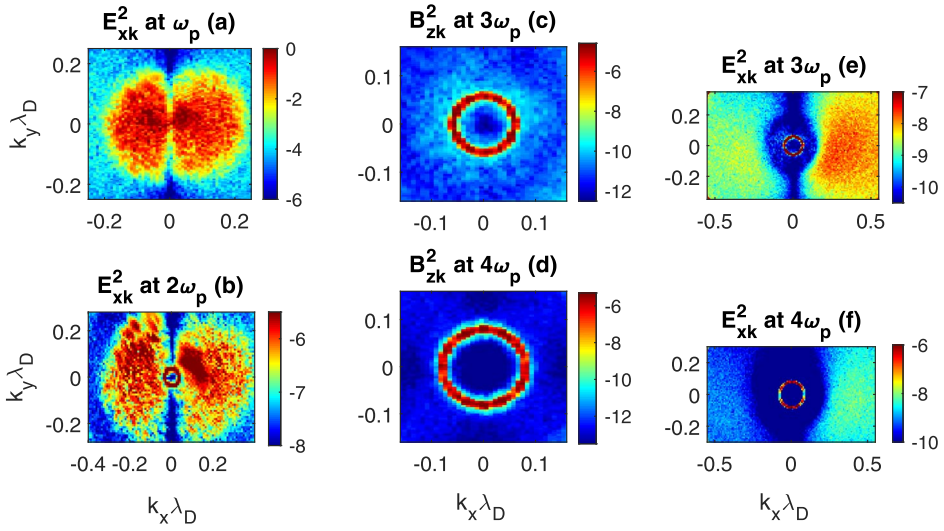

Figure 5. Inhomogeneous plasma ($\Delta N = 0.05$) at asymptotic time $\omega_p t = 7150$: wave spectra in the plane (k_x, k_y). (a) $|E_{xk}|^2$ at $\omega_k \simeq \omega_p$; the spectral domains of the waves $\mathcal{L}$ and $\mathcal{L}''$ ($k_x > 0$) are overlapped. (b) $|E_{xk}|^2$ at $\omega_k \simeq 2\omega_p$ with electric field contribution to $\mathcal{H}_2$ (central ring) and electrostatic harmonics $\mathcal{L}_2$ ($k_{2x} > 0$) and $\mathcal{L}'_2$ ($k'_{2x} < 0$). (c) $|B_{zk}|^2$ at $\omega_k \simeq 3\omega_p$: wave $\mathcal{H}_3$. (d) $|B_{zk}|^2$ at $\omega_k \simeq 4\omega_p$: wave $\mathcal{H}_4$. (e) $|E_{xk}|^2$ at $\omega_k \simeq 3\omega_p$ with electric field contribution to $\mathcal{H}_3$ (central ring) and electrostatic harmonics $\mathcal{L}_3$ ($k_{3x} > 0$) and $\mathcal{L}'_3$ ($k'_{3x} < 0$). (f) $|E_{xk}|^2$ at $\omega_k \simeq 4\omega_p$, with electric field contribution to $\mathcal{H}_4$ (central ring) and electrostatic harmonics $\mathcal{L}_4$ ($k_{4x} > 0$) and $\mathcal{L}'_4$ ($k'_{4x} < 0$). All variables are normalized. Logarithmic scales are used.

due to the waves' transformations on inhomogeneities, they exhibit scattering, broadening, and isotropization (also at earlier times). The circular rings representing the electromagnetic waves $\mathcal{H}_3$ and $\mathcal{H}_4$ can be clearly observed (Figures 5(c)–(f)).

Figures 4(b)–(c) present the time variations of the waves $\mathcal{L}_1$, $\mathcal{L}_n$, and $\mathcal{L}'_n$. It was not possible to calculate with good accuracy the energy of the waves $\mathcal{L}''$ for $\omega_p t \lesssim 4800$ as, due to Langmuir wave scattering on density fluctuations, their spectral domain largely overlaps that of the waves $\mathcal{L}$ (Figure 5(a)). Figures 4(b) and (d) show that $W_{\mathcal{L}'} \propto W_{\mathcal{H}_2} W_{\mathcal{H}_3}$ and $W_{\mathcal{H}_2} \propto W_{\mathcal{H}_3} W_{\mathcal{L}'}$ during the stage of growth $[700\text{--}2000]\omega_p^{-1}$ of $\mathcal{H}_2$, whereas $W_{\mathcal{H}_3} \propto W_{\mathcal{H}_2} W_{\mathcal{L}'}$ (Figure 4(e)) can be observed a little later but only during shorter time periods. One observes in Figures 4(d)–(e) that $W_{\mathcal{H}_2} \propto W_{\mathcal{H}_3} W_{\mathcal{L}}$ and $W_{\mathcal{H}_3} \propto W_{\mathcal{H}_2} W_{\mathcal{L}}$ are satisfied within $[5000\text{–}8400]\omega_p^{-1}$, whereas $W_{\mathcal{L}} \propto W_{\mathcal{H}_2} W_{\mathcal{H}_3}$ cannot be found; the green and red straight lines in Figure 4(e) represent linear interpolations of the oscillating products $W_{\mathcal{H}_2} W_{\mathcal{L}}$ and $W_{\mathcal{H}_4} W_{\mathcal{L}}$. Note that $W_{\mathcal{H}_2} \propto W_{\mathcal{H}_3} W_{\mathcal{L}''}$ can be observed within $[4800\text{–}7400]\omega_p^{-1}$ (Figure 4(d)) but not $W_{\mathcal{L}''} \propto W_{\mathcal{H}_2} W_{\mathcal{H}_3}$ and $W_{\mathcal{H}_3} \propto W_{\mathcal{H}_2} W_{\mathcal{L}''}$. Moreover, it appears that the process $\mathcal{L}'_3 + \mathcal{L} \longrightarrow \mathcal{H}_4$ is likely possible as $W_{\mathcal{L}} \propto W_{\mathcal{H}_4} W_{\mathcal{L}'_3}$ (Figure 4(b)) and $W_{\mathcal{L}'_3} \propto W_{\mathcal{H}_4} W_{\mathcal{L}}$ (Figure 4(c)) are fulfilled after Langmuir wave energy saturation. In turn, $W_{\mathcal{L}} \propto W_{\mathcal{H}_3} W_{\mathcal{H}_4}$ (Figure 4(b)), $W_{\mathcal{H}_3} \propto W_{\mathcal{H}_4} W_{\mathcal{L}}$ (Figure 4(e)) and $W_{\mathcal{H}_4} \propto W_{\mathcal{H}_3} W_{\mathcal{L}}$ (Figure 4(f)) are clearly observed in the same range of late times, i.e., roughly $[4800\text{–}7000]\omega_p^{-1}$, corresponding to the occurrence of the process $\mathcal{H}_3 + \mathcal{L} \longrightarrow \mathcal{H}_4$.

In conclusion, $\mathcal{H}_3$ and $\mathcal{H}_4$ can be generated by wave coalescence in spite of density fluctuations responsible for the early damping of all the Langmuir waves' energies. The dominant processes are the same as for the homogeneous plasma, i.e., $\mathcal{H}_2 + \mathcal{L}_1 \longrightarrow \mathcal{H}_3$, with $\mathcal{L}_1 = \mathcal{L}$, $\mathcal{L}'$, and $\mathcal{H}_3 + \mathcal{L}_1 \longrightarrow \mathcal{H}_4$, with $\mathcal{L}_1 = \mathcal{L}$. Note the more important role played by the beam-driven waves $\mathcal{L}$ when the plasma is inhomogeneous. To support this conclusion, some examples of cross sections of the auto- and cross-bicoherences b_c are presented in the right column of Figure 3 for $\Delta N = 0.05$, showing wave–wave interactions occurring in agreement with Figure 4.

4. Conclusion

The third and fourth electromagnetic harmonics $\mathcal{H}_3$ and $\mathcal{H}_4$ are observed in two-dimensional PIC simulations modeling the propagation of a weak electron beam generating Langmuir wave turbulence in solar wind plasmas with density fluctuations of average levels of a few percent. For comparison, the case of a homogeneous plasma with the same physical parameters, relevant to type III solar radio bursts' regions, is studied jointly. For the first time, a detailed study of the role played by different nonlinear wave coalescence processes in the generation of these harmonics is presented, and the impact of density fluctuations on these mechanisms is demonstrated.

The energy ratios $W_{\mathcal{H}_3}/W_{\mathcal{H}_2}$ and $W_{\mathcal{H}_4}/W_{\mathcal{H}_3}$ are consistent with observations of type III radio bursts. The presence of density fluctuations reduces by less than one order of magnitude the energies carried asymptotically by the electromagnetic harmonics.

It is shown that, in the homogeneous plasma, the dominant process generating the harmonic $\mathcal{H}_3$ is the coalescence of $\mathcal{H}_2$ with a Langmuir wave and, more precisely, with a backscattered wave $\mathcal{L}'$ coming from the first cascade of the electrostatic decay $\mathcal{L} \longrightarrow \mathcal{L}' + \mathcal{S}'$ and, at later times, with the forward-propagating wave $\mathcal{L}''$ produced by the second cascade $\mathcal{L}' \longrightarrow \mathcal{L}'' + \mathcal{S}''$. The same conclusions can be stated for the generation of the harmonic $\mathcal{H}_4$. Moreover, other less prominent processes occur, i.e., the coalescence of a beam-driven Langmuir wave $\mathcal{L}$ with the decay product $\mathcal{L}'_2$ ($\mathcal{L}'_3$) of the second (third) electrostatic harmonic $\mathcal{L}_2$ ($\mathcal{L}_3$) through the channel $\mathcal{L}'_2 + \mathcal{L} \longrightarrow \mathcal{H}_3$ ($\mathcal{L}'_3 + \mathcal{L} \longrightarrow \mathcal{H}_4$). There is no evidence for the coalescence process of three Langmuir waves.

When the plasma contains density fluctuations, the energies of Langmuir waves damp after saturation. Nevertheless, the harmonics $\mathcal{H}_3$ and $\mathcal{H}_4$ can be generated by wave coalescence despite the inhomogeneities randomly modifying the resonance conditions of the waves by energy transport in k-space. The dominant processes are the same as for the homogeneous plasma, i.e., the coalescence of harmonics $\mathcal{H}_2$ ($\mathcal{H}_3$) with a Langmuir wave generating $\mathcal{H}_3$ ($\mathcal{H}_4$). The role of the backscattered Langmuir waves $\mathcal{L}'$ is decisive in such process, so it should be accompanied by low-frequency emissions. The coalescence involving electrostatic harmonics could also be identified, for the generation of $\mathcal{H}_4$.

This paper sheds light on the nonlinear wave processes occurring in plasmas with random density fluctuations that are relevant to type III solar radio bursts' conditions. Understanding wave coalescence mechanisms can provide indirect information on Langmuir and ion acoustic wave turbulence, the average level of density inhomogeneities, and suprathermal electron fluxes generated in solar wind regions where harmonic waves manifest. Indeed, their presence is likely due to unusual type III beam conditions leading to the generation of intense beam-driven Langmuir waves and low-frequency emissions. The latter mostly arise from the first cascade of the electrostatic decay of beam-driven waves, which also produces backscattered Langmuir waves, whose role in the wave coalescence processes of generating higher electromagnetic harmonics $\mathcal{H}_{n>2}$ has been shown to be decisive by the present simulations. According to wave–wave resonance conditions, the coalescence $\mathcal{H}_2 + \mathcal{L}' \longrightarrow \mathcal{H}_3$ requires that the exciter beam's velocity overcomes the threshold

$$V_b \simeq c\left(2\sqrt{2} + \sqrt{3} + \frac{2}{3}\sqrt{\frac{m_e^2 c^2 (1 + 3T_i/T_e)}{m_i k_B T_{e,\max}}}\right)^{-1},$$

which, in coronal conditions with $T_{e,\max} \approx 3MK$ and $T_i/T_e \approx 1$, is around $0.17c$. This threshold lies much above the median values of type III beams in the corona as shown by recent measurements and analyses by Krupar et al. (2015; see Figure 4 therein). This condition could explain, together with the instrumental limitations reported by some authors during observations of higher harmonics in the foreshock and the solar wind (Cairns 1988; Reiner & MacDowall 2019) and with the hot plasma sources required for the second harmonic's generation (Melrose 1982), the scarcity of observations of such higher harmonic waves. Anyway, those are the signatures of the simultaneous presence of exciter beams around twice as fast as the average, of hot plasma sources, and significant low-frequency emissions.

This work was granted access to the HPC resources of IDRIS under allocation 2021-A0110510106 made by GENCI. This work was supported by the Programme National PNST of CNRS/INSU co-funded by CNES and CEA.

ORCID iDs

C. Krafft https://orcid.org/0000-0002-8595-4772

References

Bakunin, L. M., Ledenev, V. G., Kosugi, T., & McLean, D. J. 1990, SoPh, 129, 379
Brazhenko, A. I., Melnik, V. N., Konovalenko, A. A., et al. 2012, OAP, 25, 181
Cairns, I. H. 1986, JGR, 91, 2975
Cairns, I. H. 1988, JGR, 93, 858
Derouillat, J., Beck, A., Pérez, F., et al. 2018, CoPhC, 222, 351
Kliem, B., Krueger, A., & Treumann, R. A. 1992, SoPh, 140, 149
Krafft, C., & Savoini, P. 2021, ApJL, 917, L23
Krafft, C., & Savoini, P. 2022, ApJL, 924, L24
Krafft, C., Volokitin, A. S., & Krasnoselskikh, V. V. 2015, ApJ, 809, 176
Krupar, V., Kontar, E. P., Soucek, J., et al. 2015, A&A, 580, A137
Kundu, M. R. 1965, in Solar Radio Astronomy, ed. W. John (New York: Interscience)
Melrose, D. B. 1982, SoPh, 79, 173
Reiner, M. J., & MacDowall, R. J. 2019, SoPh, 294, 91
Reiner, M. J., Stone, R. G., & Fainberg, J. 1992, ApJ, 394, 340
Rhee, T., Ryu, C.-M., Woo, M., et al. 2009, ApJ, 694, 618
Takakura, T., & Yousef, S. 1974, SoPh, 36, 451
Yi, S., Yoon, P. H., & Ryu, C.-M. 2007, PhPl, 14, 013301
Yin, L., Ashour-Abdalla, M., El-Alaoui, M., Bosqued, J. M., & Bougeret, J. L. 1998, GeoRL, 25, 2609
Zheleznyakov, V. V., & Zlotnik, E. Y. 1974, SoPh, 36, 443
Ziebell, L. F., Yoon, P. H., Petruzzellis, L. T., Gaelzer, R., & Pavan, J. 2015, ApJ, 806, 237
Zlotnik, E. I. 1978, SvA, 22, 228
Zlotnik, E. Y., Klassen, A., Klein, K. L., Aurass, H., & Mann, G. 1998, A&A, 331, 1087